Spin-wave population in nickel after femtosecond laser pulse excitation

Benjamin Lenk,[1,*] Gerrit Eilers,[1] Jaroslav Hamrle,[2] and Markus Münzenberg[1]

[1]*I. Institute of Physics, University of Göttingen, 37077 Göttingen, Germany*
[2]*Centre for Advanced Innovation Technology, VSB-Technical University of Ostrava, 708 33 Ostrava-Poruba, Czech Republic*

The spin-wave relaxation mechanisms after intense laser excitation in ferromagnetic nickel films are investigated with all-optical pump-probe experiments. Uniform precession (Kittel mode), Damon-Eshbach surface modes and perpendicular standing spin waves can be identified by their dispersion $\omega(H_{ext})$. However, different to other ferromagnets $\omega(H_{ext})$ deviates from the expected behavior. Namely, a mode discontinuity is observed that can be attributed to a nonlinear process. Above a critical field the power spectrum reveals a redistribution of the energy within the spin-wave spectrum populated.

I. INTRODUCTION

Spin-wave generation and manipulation have already been demonstrated in many ways.[1] They are of great importance in magnetism-based spin-wave logic and XNOR as well as NAND gates have recently been implemented.[2] To reduce the size of potential devices, effective spin-wave pumping mechanisms are needed in ferromagnetic metallic films owning micron to nanometer characteristic magnetic length scales. Here we present a pumping mechanism using femtosecond laser excitation that allows for a large precession angle ($>3°$) after local excitation. On the other hand, the relevant length scales can be artificially selected by the design of magnonic crystals, i.e., periodically microstructured and nanostructured magnetic materials, with only very selected dynamic eigenstates.[3]

For large precession angles the equations of motion are intrinsically nonlinear. This can be used to pump energy into a certain spin-wave mode by nonlinear interaction and becomes evident, for example, in spin-wave nano-oscillators.[4–6] Given a spatial separation of two spin-torque oscillators and hence, an overlap in their spin-wave power when excited by a direct current, one finds a locking of frequencies if the frequency mismatch is below a critical value. Driven to an extreme, a steady transfer of energy from higher to lower energy modes results in Bose-Einstein condensation observed at room temperature.[7]

In the following we focus on dipolar and exchange spin-wave modes in continuous films excited by intense laser pulses, where the nature of the excited spin-wave modes is tuned by the external magnetic field. The excitation by femtosecond laser pulses has major differences as compared to methods that work in thermal equilibrium. These are, for example, Brillouin light scattering (BLS),[8] conventional ferromagnetic resonance (FMR), strip-line-based techniques like vector network analyzer[9] or spatiotemporal Kerr-effect-based FMR used to study spin-wave modes.[10] Our technique works in space and time-resolved manner and the detection process owns no k selectivity *a priori*. Yet, the strongest difference to resonant techniques is the broadband excitation in the spin system,[11,12] by which all magnetic modes are excited. However, only resonant modes contribute to the signal coherently and can be detected while others appear as noncoherent background. A further advantage is the contact free, very local excitation and detection which simplifies the testing of various samples and structured media.

We make the very unusual observation that below a critical magnetic field two dominant spin-wave modes are excited, whereas above the critical field, they merge into one single mode. We shall also see that intrinsic to the experimental method used, surface modes are preferentially excited if the sample thickness considerably exceeds the penetration depth of the laser field.

In general, magnetic precessional motion can have dipolar and exchange spin-wave character and can be described as follows. Starting from the free-magnetic energy density, the Landau-Lifshitz equation of motion for the magnetization vector *M* yields a theoretical dispersion describing the uniform precession (also referred to as the Kittel mode) in the macrospin approximation[13]

$$\left(\frac{\omega_k}{\gamma\mu_0}\right)^2 = H_x\left(H_x + M_S - \frac{2K_z}{\mu_0 M_S}\right), \qquad (1)$$

where $\mu_0 M_S$ is the saturation magnetization (being $=659$ mT for nickel), the only free parameter K_z accounts for the effective anisotropy in the out-of-plane direction, and H_x is the component of the external field projected to the sample plane. Damon and Eshbach solved the equation of motion accounting for Maxwell's equations in the magneto-static limit and adequate boundary conditions yielding the dispersion for long-wavelength surface modes, so-called Damon-Eshbach (DE) modes,

$$\left(\frac{\omega_{DE}}{\gamma\mu_0}\right)^2 = H_x(H_x + M_S) + \frac{M_S^2}{4}[1 - \exp(-2k_{DE}d)]. \quad (2)$$

Here, d is the film thickness and $k_{DE} \perp M_S$ denotes the wave vector of the magnetostatic surface wave. An analogous approach in Ref. 14 yields dispersion characteristics taking into account exchange interaction as well as anisotropy. In thin magnetic layers one finds a quantization of the wave vector perpendicular to the sample plane and in analogy to Eq. (1) one can give a dispersion describing the exchange-dominated perpendicular standing spin waves (PSSWs),
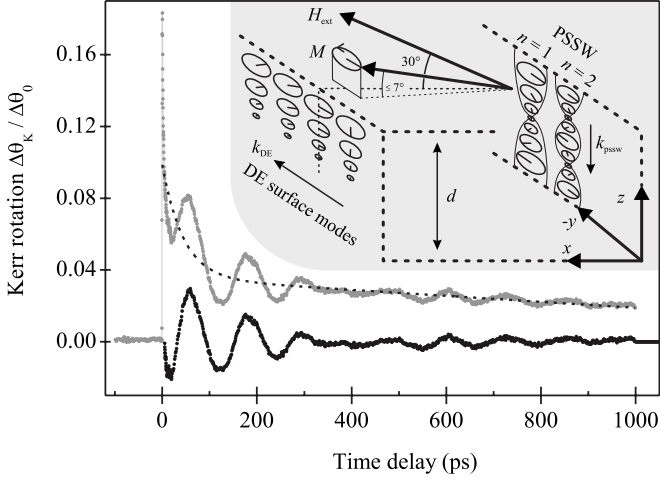
FIG. 1. Time-resolved measurement of the pump-induced change in the Kerr rotation (light gray) and the fitted background (dashed line) that is subtracted to yield the residual oscillation (black). The data set shown has been recorded at a nickel thickness of 80 nm under an external field of 140 mT. A large angle of precession as high as 3° is observed. Inset: schematic representation of spin-wave modes in a continuous ferromagnetic film of thickness d. Local amplitude and phase of the dynamic magnetization $m(t)$ are illustrated. Shape anisotropy accounts for mainly in-plane alignment of the magnetization $M = M_S + m(t)$.

$$\left(\frac{\omega_{PSSW}}{\gamma\mu_0}\right)^2 = \left(H_x + \frac{2A}{\mu_0 M_S}k_{PSSW}^2\right)$$
$$\times \left(H_x + M_S - \frac{2K_z}{\mu_0 M_S} + \frac{2A}{\mu_0 M_S}k_{PSSW}^2\right). \quad (3)$$

Therein, A is the exchange constant and $k_{PSSW} = n\pi d^{-1}$ is the quantized wave vector in out-of-plane (i.e., z) direction attributed to a given order n of the PSSW. A schematic of the different magnetic modes is given in the inset of Fig. 1 where the Kittel mode is not explicitly drawn, as both PSSW and DE modes result in the uniform precession in the limit $k_{PSSW} \to 0$ (i.e., $n=0$) and $k_{DE} \to 0$, respectively.

II. EXPERIMENT

The samples consist of polycrystalline nickel films with thicknesses of up to 220 nm. The thickness dependence of the occurring modes is measured on a wedge-shaped sample to perform all measurements on one specimen. It was prepared by electron-beam evaporation in ultrahigh vacuum under a base pressure of 5×10^{-10} mbar. A linearly moving shutter was used to produce a nickel wedge with thickness 20 nm $\leq d \leq$ 220 nm on a Si(100) substrate and in order to prevent oxidation, the ferromagnetic layer was capped with 2 nm of copper.

For the experiments we use an approach in the time domain, i.e., an all-optical pump-probe setup as previously described in Ref. 15. An ultrashort laser pulse with 60 fs duration and $\lambda_c = 810$ nm central wavelength excites the saturated sample and at a variable time delay τ a second laser pulse with the same characteristics but 5% of the intensity

probes the time-resolved magneto-optical Kerr effect (TRMOKE).[16–18] Therewith, spin dynamics in the femtosecond regime can be detected, where electronic excitations lead to a demagnetization and subsequent relaxation into the initial state via scattering of high-energy to low-energy spin waves.[11] The processes that initially quench the magnetization in the first few picoseconds are subject to ongoing discussions[19] but can be modeled quite successfully in some detail.[12] Here in focus are oscillations on a time scale from 30 ps to 1 ns. We shall see that all modes corresponding to Eqs. (1)–(3) can be optically excited in a thin ferromagnetic film. In a simplified picture the mechanism can be regarded as an effective-field pulse which stems from the heat-induced change in the sample's anisotropy and local exchange field upon absorption of the pump pulse.[20] Therefore, to promote magnetic precession of the Kittel mode, the external field was tilted by 30° out of plane thus giving rise to an angle between sample plane and the effective internal field $H_i \| M_S$. For an external field of $\mu_0 H_{ext} = 150$ mT, which is the maximum used in the experiments, we calculated a rotation of 7° of H_i out of plane due to the Zeeman term in balance with the shape anisotropy (see also Fig. 1). The angle is rather small and thus, its influence can be neglected for simplicity. Hence, in the analytical expression of the spin-wave modes we assume H_i and M_S to be in plane. The data presented here have all been recorded with the field applied under 30°. Please see the supplemental materials section for experiments at other angles and a detailed hysteresis analysis.[26]

III. RESULTS AND DISCUSSION

In order to obtain the precession frequencies from the time-dependent MOKE spectra, the incoherent background owing to phonons and magnons is subtracted. This procedure is demonstrated in Fig. 1 with a single measurement recorded at $\mu_0 H_{ext} = 140$ mT and $d = 80$ nm. After subtraction of the background (black data points in Fig. 1), Fourier transformation of the $M(\tau)$ curves yields peaks in the oscillations' power spectra. For a given thickness d, the external field is varied between 0 and 150 mT, resulting in a change in amplitude and frequency of the oscillation. The position of the corresponding peaks in the frequency domain is determined for each such set of measurements and plotted versus $\mu_0 H_{ext}$.

Shown in Fig. 2 are power spectra recorded on different nickel thicknesses, revealing up to three precessional modes of different origin. In the upper row the Fourier power spectra for a given thickness are plotted in a color map as calculated from the $M(\tau)$ curves (the Fourier transformation of the data from Fig. 1 is marked with a vertical gray line). In the bottom row all spectra have been normalized by their respective maximal fast Fourier transform power to give a better overview of mode evolution. The data points represent the peak positions and included as solid lines are the fitted theoretical frequency dispersions [Eqs. (1)–(3)] of the various modes, which have been used to attribute the branches to the Kittel mode, the DE surface mode, as well as the PSSW mode with $n=1$.

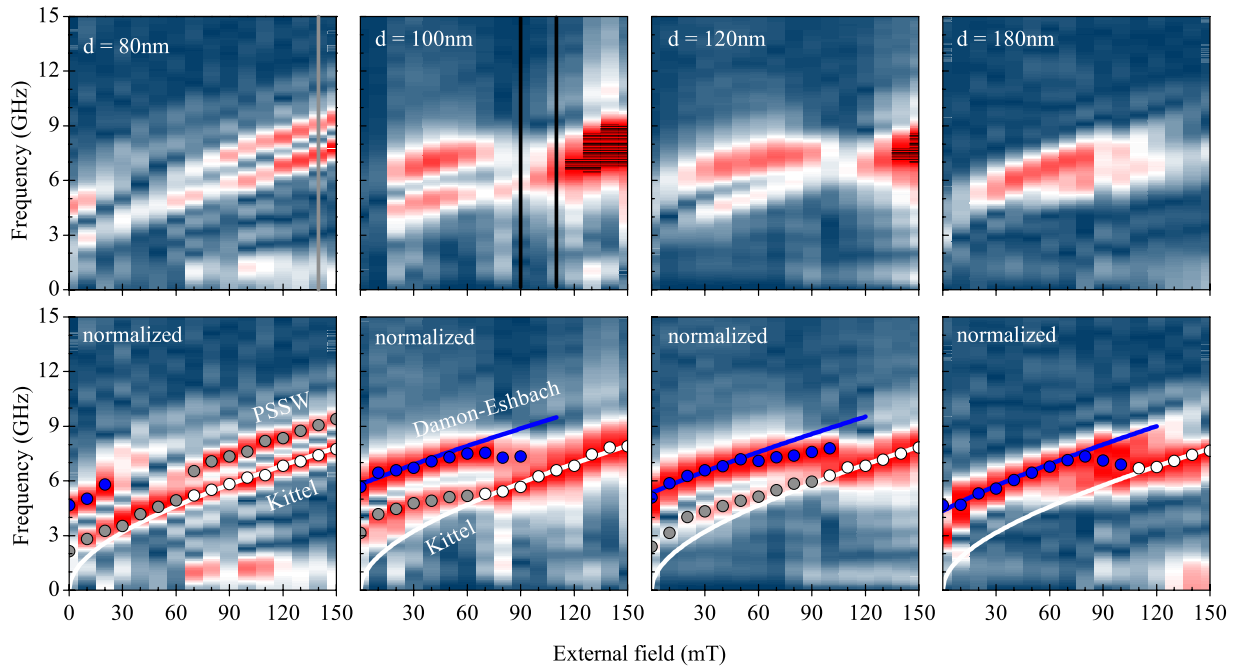Analysis of the thickness-dependent occurrence of the different magnetic modes yields the results depicted in Fig. 3.

FIG. 2. (Color online) Spin-wave power spectra of thin nickel films with $d=80-180$ nm. Magnetic oscillations are observed after optical excitation (top plots) and normalization yields frequency branches (bottom plots) that can be attributed to uniform precession (white points), magnetostatic surface waves (blue points), as well as perpendicular standing spin waves (gray points). Solid lines represent theory according to Eqs. (1)–(3). The vertical gray line at 80 nm of nickel corresponds to the data set from Fig. 1, vertical black lines for 100 nm denote Fourier spectra analyzed in Fig. 4. Please note the mode discontinuity around $\mu_0 H_{ext}=90$ mT for $d>80$ nm.

For a given external field of 50 mT the observed frequencies have been extracted and the aforementioned identification of Kittel, PSSW, and DE modes is confirmed. Both the Kittel mode (black) and the PSSW (gray) display the expected evolution with the thickness: while the frequency of uniform precession ω_K remains unchanged, the frequency of the PSSW reduces. Being proportional to d^{-2} it approaches ω_K in accordance to literature.[21,22]

The DE modes (blue lines and squares in Fig. 3) have been predominantly studied with BLS.[23] We find from our experiment that they are first excited at a nickel thickness of 80 nm. There, they are only present at low external fields but for thicker nickel layers these modes dominate the spin-wave dynamics over a wider field range up to $\mu_0 H_{ext}$ $=90$ mT. This is due to the excitation mechanism and its relevant length scales: sample thickness d and optical penetration depth Λ_{opt} (i.e., penetration depth of the electrical field at optical frequencies which evaluates to $\lambda/[2\pi\mathfrak{J}(N)]$ ≈ 30 nm, where N is the complex refractivity index). Calculations that show our experiments' sensitivity to magnetic modes in the top 15 nm of the ferromagnet can be found elsewhere.[24] The magnetic excitation depth is governed by the penetration of the laser field and energy is deposited in form of an initial disarrangement of spins.[11] This energy will very effectively excite eigenmodes with similar spatial profile and thus, by choosing a thickness $d\gg\Lambda_{opt}$, the resulting strong asymmetry will make DE surface modes the favored relaxation channel. Consequently, the appearance of the DE modes is based on the fact that they own an amplitude profile with the maximum at the surface, decaying exponentially into the film. Herein lies a strong analogy to surface acoustic

waves excited with laser pulses, which can be used to determine elastic properties of surface layers.[25]

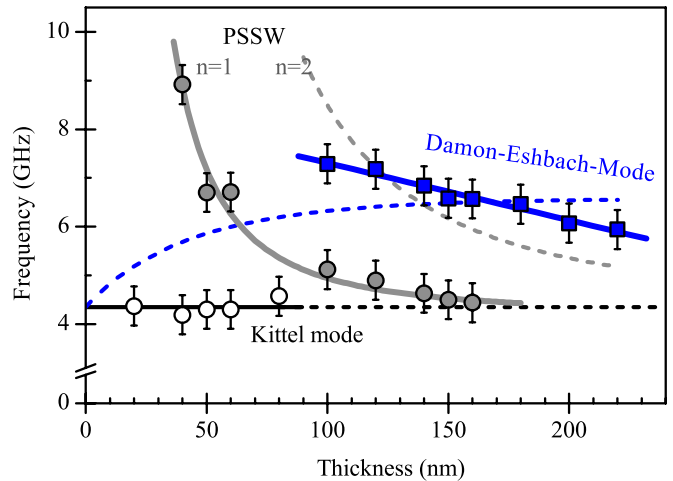Assuming a propagation direction perpendicular to the magnetization $(k_{DE}\perp M_S, H_{ext})$ the dispersion [Eq. (2)] can

FIG. 3. (Color online) Spin-wave modes at $\mu_0 H_{ext}=50$ mT for varying thickness d. Below 40 nm only the uniform precession (white points, black line) is observed, which does not change in frequency for increasing d. Perpendicular standing spin waves with $n=1$ can also be identified (gray) and fit well to the expected d^{-2} behavior (Ref. 21). PSSW of second order are not observed (dashed gray line), instead Damon-Eshbach surface waves (blue) are excited. The blue dashed line represents the DE dispersion [Eq. (2)] with $k_{DE}=1$ μm^{-1} and reveals that the DE wave vector is not constant in our experiment (the solid blue line is a guide to the eyes).
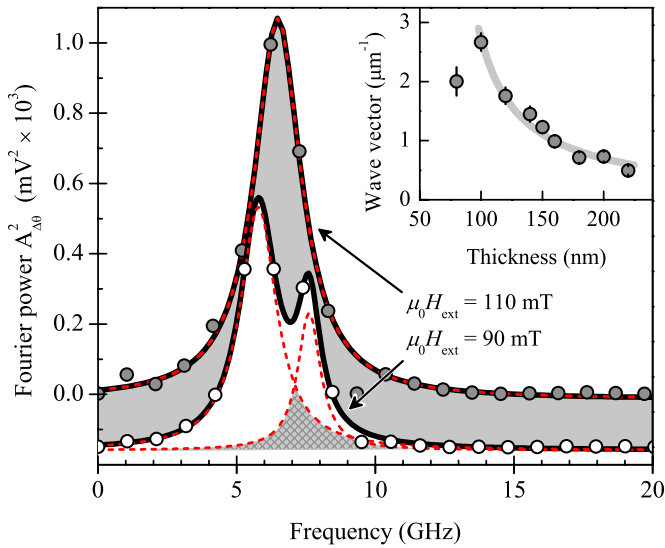
FIG. 4. (Color online) Gray and white points denote the Fourier power $A_{\Delta\theta}^2$ as calculated from the time-resolved MOKE measurements at $d=100$ nm, $\mu_0 H_{ext}=110$ mT, and 90 mT, respectively. Solid and dashed lines represent Lorentz peaks which where fitted to the data. The expected linewidth in nickel is larger than 1 GHz and as a result, possible mode locking leads to the population of only a single mode at 110 mT if the overlap indicated by the hatched area is increased. Additionally, the mutual intensity is strongly increased. In the inset, the dependence of the Damon-Eshbach wave vector on the thickness is given, where the solid gray line is a guide to the eyes (see text also).

be used to determine the wave vector k_{DE}. In the inset of Fig. 4 the respective quantitative analysis of the Damon-Eshbach modes is given. From the fits one obtains wave vectors in the inverse micrometer range, corresponding to wavelengths of about 3 μm. We find that the product $k_{DE}d$ entering Eq. (2) is not constant but that the relation $k_{DE}=(d-d_0)^{-1}$ holds with $d_0=66(4)$ nm (solid gray line in the inset of Fig. 4). The divergence of k_{DE} around that value supports our earlier interpretation. An asymmetry between film thickness and optical excitation depth is needed to give rise to dipolar spin waves in contrast to exchange-dominated spin waves with rather high k. In other words, the parameter d_0 can be considered an onset thickness above which the dipolar interaction comes into play. In general, our understanding of the selection of the DE wave vector is not fully developed. However, we can exclude that the laser spot sizes of pump (60 μm) or probe (20 μm) enforce a selection since the observed DE wavelengths are on the order of only very few microns. A tentative reduction in the probe beam diameter to 14 μm did not result in a change in k_{DE}. The pump beam on the other hand is only present for a very short period of time. The formation of a boundary condition resulting from the demagnetized spot and a selection of the k vector whose wavelength is related to multiples of the demagnetization spot is therefore improbable. Most importantly the characteristic thickness dependence of k_{DE} is a counter indication for the latter model.

Another possibility for the formation of the Damon-Eshbach mode is a periodic inhomogeneity of the magneti-zation intrinsic to the ferromagnetic film. The supplemental data include hysteresis curves for various film thicknesses which will be discussed in the following.[26] The coercive fields are around 20 mT, which is well below the area of interest. It is clear that if magnetic domains appeared, their irregularity would destroy any coherent and well-defined Damon-Eshbach mode. In the experiments the TRMOKE spectra have been measured by applying 150 mT and subsequently reducing the magnetic field after saturation of the sample. However, periodic ripple patterns are known to appear in materials with small crystallites to adapt the direction of the local anisotropy. Typically in the few microns range the deviation of the magnetization direction can be up to a few 10°.[27] The ripple patterns are known to change periodicity depending on the film thickness and could explain the longer wavelengths observed for thicker Ni films. Still, certain difficulties in this model arise that do not match some of our observations. First, the region of existence terminated by the critical field does not match the saturation field values that are typically much lower. Also, we observe a constant k vector over a wide field region, indicating that the periodicity of the (hypothetical) ripple pattern is almost field independent. This opposes experimental findings by Gentils *et al.* who found a strong dependence of the ripple periodicity on the applied field.[27] Further experiments using Kerr microscopy performed in collaboration with the IFW at Dresden did not yield any evidence for ripple patterns. Instead, rather large domain structures above 15 μm dominate the magnetization reversal. A periodic variation in the magnetization can thus be rather only small in angle but also too small then to form the periodic potential for the selection of the k vector of the Damon-Eshbach standing wave. Moreover, the periodicity of the ripple pattern is found along the direction of the applied field while the Damon-Eshbach modes propagate perpendicular to that. Such a periodic magnetic pattern could only form a periodic boundary condition for the backward volume mode. The respective energy when compared to the Kittel mode should be lower, which is not consistent with our data. At this stage we conclude that we cannot totally exclude an effect of an inhomogenous magnetization but considerable observations point against such an interpretation.

As described, the DE mode dominates the spectra up to critical fields as high as $\mu_0 H_{crit}=90$ mT. Around that value, an explicit deviation from the theoretical dispersion arises (blue line and points in the bottom row of Fig. 2). A distinct modification of the DE mode intensity takes place which—for sufficiently high fields—ultimately results in a peculiar characteristic evident in Fig. 2. Namely, the DE mode merges into the Kittel mode. This leads to a very strong increase in the total Fourier power, i.e., precession amplitude, as seen in the non-normalized data (upper row of Fig. 2). The propagating surface mode seems to lock to the frequency of the Kittel and PSSW modes for magnetic fields higher than $\mu_0 H_{crit}$. Above that value, the peaks can be attributed to the dispersion of the uniform precession by Eq. (1). The fits (white lines) yield values for the effective anisotropy K_z around 50 kJ m^{-3} showing no monotonous trend with the thickness.

The idea to explain the merging of both modes is based on the alternating magnetic field that the stationary precession
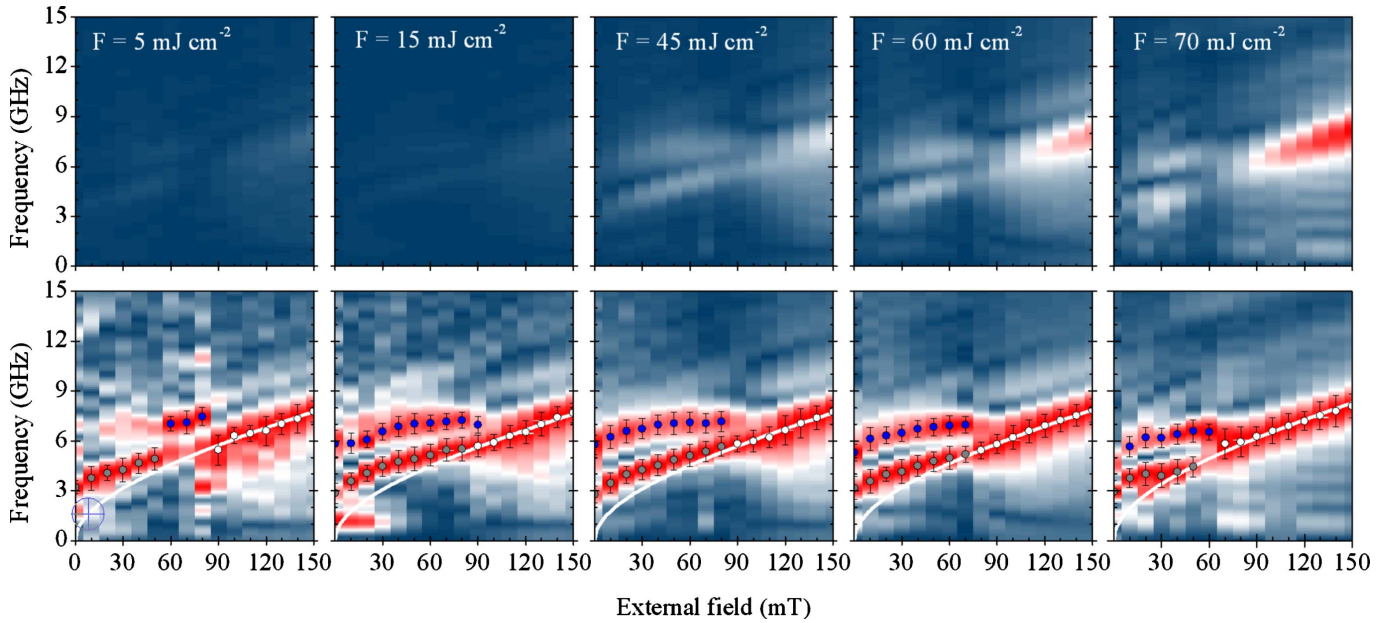
FIG. 5. (Color online) Fourier power spectra for different pumping fluences $F = 5–70$ mJ cm^{-2} with $d = 150$ nm. The identification of modes corresponds to Fig. 2 and the color scale in the top row (not normalized plots) is the same for every spectrum to reveal the fluence dependence of the precession amplitude. One observes a strongly increasing amplitude of the uniform precession with increasing fluence, whereas the bottom row (normalized data) shows a small shift of the critical field toward lower values, which will be detailed in Fig. 6.

of the magnetization generates. In this respect, the absolute value of the amplitude is of great interest. It can be derived from the dynamic magnetization by calibration of the experiment for a given saturation magnetization: A comparison of the magneto-optical signal at zero time delay with and without pump-induced demagnetization at $F = 70$ mJ cm^{-2} and $\mu_0 H_{ext} = 150$ mT. This results in a precessional amplitude of $4.6\% \times \mu_0 M_S$ corresponding to an angle of 3°. One calculates an absolute value of 30 mT which would provide a rather strong coupling field. Thus, another hypothesis to understand the observation is a locking of the DE mode to the $k = 0$ homogenous precession originating from an energy transfer between the two dynamic modes. Only if the propagating surface waves would couple to the alternating field of the Kittel mode the amplitude of the magnetic precession could be that drastically increased.

A reasonable starting point to test this general idea is to draw parallelities to a model by Slavin and co-workers. They proved that phase locking of spin-torque nano-oscillators can take place.[4] In their publication, the authors use a nonlinear set of equations of motion for two coupled oscillators and can explain the experimental results presented in Refs. 5 and 6. Once the free-running frequency mismatch between the two oscillators is smaller than a threshold value Δ_{max} [Eq. (9) in Ref. 4], they phase lock to a mutual frequency. The mechanism is twofold: coupling can be either mediated by spin waves radiated into a common magnetic layer or a dipole field created by the oscillators. Either way, one of the crucial parameters is the spatial separation a of the two contacts, tuning the overlap of spin-wave power in real space (Fig. 1 in Ref. 4).

Transferring these findings to our observation, we could speculate that an increased overlap of the magnetic modes in Fourier space leads to a sudden interaction such that locking

takes place. Figure 4 illustrates this hypothesis: two Fourier spectra from measurements recorded on nickel with a thickness of 100 nm are shown. At $\mu_0 H_{ext} = 90$ mT clearly two precessional modes can be distinguished, whereas at $\mu_0 H_{ext} = 110$ mT only one smooth peak with nearly identical width is found. The two modes observed, namely, uniform precession and DE surface waves, are separated in Fourier space by several gigahertzs at low external fields. However, if $\mu_0 H_{ext}$ is increased in the experiment, the separation reduces and at one point approaches the value of the linewidth, which implies an overlap in the frequency domain (hatched area in Fig. 4). Above a threshold overlap the frequencies seem to lock and the two modes cannot be distinguished anymore. Moreover, a single smooth peak in the Fourier spectrum is observed. Concerning the evolution with increasing magnetic field, a steplike change in the DE frequency is apparent in the Fourier spectra in Fig. 2 and hence, the term mode locking seems justified.

Equivalent to the damping time constant τ_α in the time domain is the linewidth in the Fourier domain. From τ_α apparent in the time-resolved MOKE spectra one expects the width of the peak after Fourier transformation to be $(\pi\tau_\alpha)^{-1}$ at 50% of maximum power (full width half maximum). For nickel the expected line width therefore is 1.1 GHz, using $\tau_\alpha = 300$ ps, which has been extracted from the time-resolved spectra. Due to the strong damping in nickel (implying a rather large linewidth) considerable overlap can occur. The interplay with H_{ext} tuning the DE and Kittel frequency mismatch leads to possible phase locking (see Fig. 4). Normally, the synchronization time of two oscillators depends on their interaction strength. We do not observe any hints for delayed synchronization in our data which is a counter indication for this hypothesis.[26] However, also significant differences to the analogy to two coupled oscillators come into play. First, the
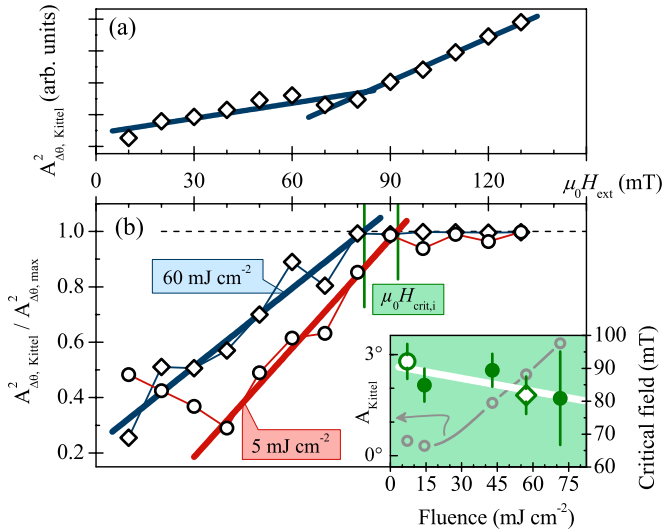
FIG. 6. (Color online) (a) Threshold behavior of the Fourier power $A^2_{\Delta\theta,\mathrm{Kittel}}$ of the Kittel mode. The external magnetic field can be used tune the observed characteristics between dipolar surface waves and uniform precession. (b) Determination of the critical magnetic field $\mu_0 H_{\mathrm{crit}}$ for different fluences $F = 5$ mJ cm^{-2} and 60 mJ cm^{-2}, respectively. $A^2_{\Delta\theta,\mathrm{Kittel}}$ is plotted after normalization to the maximum of the respective Fourier spectrum for a given external field, $A^2_{\Delta\theta,\mathrm{max}}$. The result can be regarded as a measure of mode population and a linear increase is found prior to saturation. The critical field can be extracted as depicted by the vertical green lines. In the inset, corresponding results for all fluences are included, giving a clear trend toward smaller $\mu_0 H_{\mathrm{crit}}$ for increasing F. Additionally, the Kittel amplitude as induced by different pump fluences is shown for $\mu_0 H_{\mathrm{ext}} = 150$ mT (gray points).

different excitation mechanism using optical pump pulses ensures the same initial phase which simplifies a synchronization. Second, in the spin-wave picture after laser excitation in the hot disordered ferromagnet, a broad spectrum of spin waves is present. By the alternating field of the Kittel mode the population of the Damon-Eshbach state with the wave vector k previously found at lower fields is hindered. Only spin waves synchronized with the frequency of the Kittel mode can be populated in the relaxation process. This relaxation happens very fast and takes place within 30 ps.[11] In this context, the high energy of the pump pulses is of great importance. It is delivered on ultrafast time scales pushing the system far out of equilibrium and must be considered when discussing the effects observed.

A test for our hypothesis based on nonlinearity is the influence of the (optical) pumping power that excites the magnetization dynamics. Corresponding experiments were performed on a separate continuous nickel film which was 150 nm thick and was prepared as described above. For the measurements, the pumping fluence was varied over one decade ranging from 5 to 70 mJ cm^{-2}. The resulting Fourier power spectra are presented in Fig. 5 and reveal that the nature of the magnetic modes excited by the pump pulses does not significantly change. To give a better insight into the fluence dependence, all power spectra in the top row are identically color scaled. This shows an increase in the spin-wave amplitude with the fluence (from left to right) as expected when

considering the heat-induced disorder triggering the oscillation.[20] This increase is quantitatively given in the inset of Fig. 6(b), where the Kittel amplitude at $\mu_0 H_{\mathrm{ext}} = 150$ mT has been plotted versus the pumping fluence (gray points).

A feature of Fig. 5 that requires a closer look is the somewhat changing critical field for the transition from surface to uniform characteristics. Figure 6(b) details the corresponding analysis and gives the respective results in the inset. Starting from the fit of the Kittel dispersion [Eq. (1)] to the data (white lines in the bottom row of Fig. 5) the amplitude of the Kittel mode for each magnetic field is extracted from the data. In the normalized case, this amplitude equals 1 if $H_{\mathrm{ext}} > H_{\mathrm{crit}}$ and below the critical field a monotonous, in good approximation linear behavior is found. By a linear fit, the point at which the Kittel amplitude reaches 1, i.e., above which the Kittel mode is the dominant mode of precession, can be determined. We define this field value as the critical field H_{crit} [also marked by vertical lines in Fig. 6(b)]. The above described procedure is explicitly given in Fig. 6(b) for the fluences 5 mJ cm^{-2} and 60 mJ cm^{-2}, respectively. In the inset the overall decrease in $\mu_0 H_{\mathrm{crit}}$ for increasing F is shown. Together with the thresholdlike onset of the population of the uniform precession in Fig. 6(a) and the accompanying rapid increase in precession amplitude our initial hypothesis of a nonlinear transfer of energy seems to speak in favor of the mode coupling.

IV. CONCLUSION

In conclusion, we have identified the excitation of the uniform precession (Kittel mode) as well as magnetostatic surface waves (DE mode) in asymmetrically pumped nickel films. Below a critical magnetic field H_{crit} the dipolar DE modes dominate the precession, whereas a steplike feature in the dispersion $\omega_{\mathrm{DE}}(H_{\mathrm{ext}})$ indicates the population of the $k = 0$ mode above H_{crit} (Fig. 2). The observation of the DE surface waves for $H_{\mathrm{ext}} < H_{\mathrm{crit}}$ can be understood by considering the optical excitation mechanism. A concept was developed taking into account the amplitude profile of the DE mode as well as the asymmetric excitation profile stemming from the laser pump pulses. However, the exact understanding of the DE wave vector is a challenge still to be met. The possibility of a periodic magnetic ripple pattern that imposes its periodicity onto the wave vector has been discussed. We tried to explain the transition from a well-defined DE mode to a uniform precession mediated by the external field above a critical-field value of $H_{\mathrm{ext}} > H_{\mathrm{crit}}$ and we have pinpointed possible mechanisms. Only a nonlinear process allows to explain the dependence of the transition field H_{crit} on the pumping power. In this context the high energy of the pump pulses driving the system far out of equilibrium leading to rather large precession angles should be mentioned, which is the most important experimental finding. In essence, the population of either the Kittel or the DE mode can be tuned by both the external field and the pumping fluence. Understanding the underlying mechanism might prove crucial on the way to spin-logic devices, especially with the interconversion of electrical, optical, or magnetic signals in mind.

ACKNOWLEDGMENTS

*Corresponding author. blenk@gwdg.de

[1] S. O. Demokritov, A. A. Serga, A. André, V. E. Demidov, M. P. Kostylev, B. Hillebrands, and A. N. Slavin, Phys. Rev. Lett. **93**, 047201 (2004).

[2] T. Schneider, A. A. Serga, B. Leven, B. Hillebrands, R. L. Stamps, and M. P. Kostylev, Appl. Phys. Lett. **92**, 022505 (2008).

[3] H. Ulrichs, B. Lenk, and M. Münzenberg, Appl. Phys. Lett. **97**, 092506 (2010).

[4] A. N. Slavin and V. S. Tiberkevich, Phys. Rev. B **74**, 104401 (2006).

[5] S. Kaka, M. R. Pufall, W. H. Rippard, T. J. Silva, S. E. Russek, and J. A. Katine, Nature (London) **437**, 389 (2005).

[6] F. B. Mancoff, N. D. Rizzo, B. N. Engel, and S. Tehrani, Nature (London) **437**, 393 (2005).

[7] V. E. Demidov, O. Dzyapko, S. O. Demokritov, G. A. Melkov, and A. N. Slavin, Phys. Rev. Lett. **100**, 047205 (2008).

[8] J. Jorzick, S. O. Demokritov, C. Mathieu, B. Hillebrands, B. Bartenlian, C. Chappert, F. Rousseaux, and A. N. Slavin, Phys. Rev. B **60**, 15194 (1999).

[9] S. Neusser, B. Botters, and D. Grundler, Phys. Rev. B **78**, 054406 (2008).

[10] M. J. Pechan, C. Yu, R. L. Compton, J. P. Park, and P. A. Crowell, J. Appl. Phys. **97**, 10J903 (2005).

[11] M. Djordjevic and M. Münzenberg, Phys. Rev. B **75**, 012404 (2007).

[12] U. Atxitia, O. Chubykalo-Fesenko, J. Walowski, A. Mann, and M. Münzenberg, Phys. Rev. B **81**, 174401 (2010).

[13] M. Farle, Rep. Prog. Phys. **61**, 755 (1998).

[14] B. A. Kalinikos and A. N. Slavin, J. Phys. C **19**, 7013 (1986).

[15] M. Djordjevic, G. Eilers, A. Parge, M. Münzenberg, and J. S. Moodera, J. Appl. Phys. **99**, 08F308 (2006).

[16] E. Beaurepaire, J.-C. Merle, A. Daunois, and J.-Y. Bigot, Phys. Rev. Lett. **76**, 4250 (1996).

[17] G. Ju, A. Vertikov, A. V. Nurmikko, C. Canady, G. Xiao, R. F. C. Farrow, and A. Cebollada, Phys. Rev. B **57**, R700 (1998).

[18] M. van Kampen, C. Jozsa, J. T. Kohlhepp, P. LeClair, L. Lagae, W. J. M. de Jonge, and B. Koopmans, Phys. Rev. Lett. **88**, 227201 (2002).

[19] B. Koopmans, G. Malinowski, F. Dalla Longa, D. Steiauf, M. Fähnle, T. Roth, M. Cinchetti, and M. Aeschlimann, Nature Mater. **9**, 259 (2009).

[20] Y. Liu, L. R. Shelford, V. V. Kruglyak, R. J. Hicken, Y. Sakuraba, M. Oogane, Y. Ando, and T. Miyazaki, J. Appl. Phys. **101**, 09C106 (2007).

[21] M. H. Seavey and P. E. Tannenwald, Phys. Rev. Lett. **1**, 168 (1958).

[22] From the fit in Fig. 3 (solid gray line) the exchange constant $A = 6.9(5)$ pJ m^{-1} was extracted.

[23] P. Grünberg, C. M. Mayr, W. Vach, and M. Grimsditch, J. Magn. Magn. Mater. **28**, 319 (1982).

[24] J. Hamrle, J. Pistora, B. Hillebrands, B. Lenk, and M. Münzenberg, J. Phys. D: Appl. Phys. **43**, 325004 (2010).

[25] A. Neubrand and P. Hess, J. Appl. Phys. **71**, 227 (1992).

[26] See supplementary material at http://link.aps.org/supplemental/10.1103/PhysRevB.82.134443 for additional details.

[27] A. Gentils, J. N. Chapman, G. Xiong, and R. P. Cowburn, J. Appl. Phys. **98**, 053905 (2005).